Nanoscale

COMMUNICATION

View Article Online
View Journal | View Issue

Cite this: *Nanoscale*, 2017, **9**, 7703

Received 14th March 2017,
Accepted 19th May 2017

DOI: 10.1039/c7nr01826f

rsc.li/nanoscale

Multistage extraction platform for highly efficient and fully continuous purification of nanoparticles†

Yi Shen,‡[a] Nopphon Weeranoppanant, §‡[a] Lisi Xie,[a] Yue Chen,[b] Marcella R. Lusardi,[c] Joseph Imbrogno,[a] Moungi G. Bawendi*[b] and Klavs F. Jensen *[a,c]

This paper presents a fully-continuous novel liquid–liquid-extraction (LLE) platform for the purification of nanoparticles. The use of multistage operation enhances the purity of the final stream without the expense of high solvent consumption. Two case studies, purification of CdSe quantum dots in organic solvent and that of gold nanoparticles in water, demonstrate that the LLE platform is versatile, non-destructive, and highly efficient.

In the past decade, nanoparticles in various forms and compositions have been extensively studied. A significant amount of these emerging materials have been commercialized in areas such as displays,[1] catalysis[2] and personal care.[3] To meet the growing industrial demand, much work has focused on transitioning from batch to flow preparation of metal, oxide and semiconductor nanoparticles.[4–10] Purification steps are required to remove impurities as well as unreacted precursors in order to transform as-synthesized nanoparticles to their product form. To the best of our knowledge, only a few studies have been conducted with in-line purification of nanoparticles, which is essential to achieving fully continuous production of these materials.

There are well-established batch processes for nanoparticle purification, including those based on polarity, electrophoresis, and size differences between the impurity and nanoparticles.[11] These methods encounter technical challenges and losses in purification efficiency when converted directly into flow. For example, the widely-used precipitation/redissolution (PR) method involves solid formation that may cause clogging in a flow system. Jeong's group pioneered the use of free-flow electrophoresis to purify semiconductor nanoparticles (quantum dots) on a microfluidic chip.[12] However, the separation efficiency and particle yield were lower than those for the batch process. Recently, they improved the purification efficiency and the yield by using porous electrodes in the flow channel.[13] As opposed to their previous work, this technique required two additional washing steps to purify and recover the particles on the electrodes, which makes the process semi-continuous. Hutchison *et al.* applied diafiltration, a size-based separation technique, to continuously purify gold nanoparticles in aqueous solution.[14] This technique is limited by the development of membrane materials, particularly when the membranes are not compatible with organic solvents in which nanoparticles are prepared.

One possible alternative is liquid–liquid extraction (LLE). LLE, a polarity based technique, has been well studied as a batch method for nanoparticle purification.[15] LLE allows impurities to be selectively extracted into one phase while the desired nanoparticles remain in the other immiscible phase.[15] The major advantages of LLE are easy scale-up, non-destructive operation and minimal energy requirements.[16] In this work, we design and use the LLE platform to perform continuous purification of nanoparticles. The platform is reconfigurable into either one or multiple stages. Each stage features tubing with segmented flow for mass transfer between phases and a membrane for separation of the two phases. The tubing allows a controlled residence time for complete extraction of precursors from their original phase to the other immiscible phase. A mixed biphasic flow in micro- or submillimeter-channels typically has a well-defined flow pattern with a large interfacial area,[16] providing a reproducible and fast extraction rate. Generally, at this submillimeter scale, the two phases are mixed into the tubing with different patterns ranging from parallel to segmented to irregular droplet, depending on flow properties and tube dimensions.[17,18] Here, a segmented flow is obtained with high mass transfer rate provided by the high surface-to-volume ratio and the enhanced mass convection inside each droplet.[19,20] A residence time of 10 s to 20 s inside

[a]*Department of Chemical Engineering, Massachusetts Institute of Technology, Cambridge, MA, 02139, USA. E-mail: kfjensen@mit.edu*
[b]*Department of Chemistry, Massachusetts Institute of Technology, Cambridge, MA, 02139, USA. E-mail: mgb@mit.edu*
[c]*Department of Materials Science and Engineering, Massachusetts Institute of Technology, Cambridge, MA, 02139, USA*
†Electronic supplementary information (ESI) available. See DOI: 10.1039/c7nr01826f
‡These authors contributed equally.
§Present address: Department of Chemical Engineering, Faculty of Engineering, Burapha University, Chonburi, Thailand, 20130.

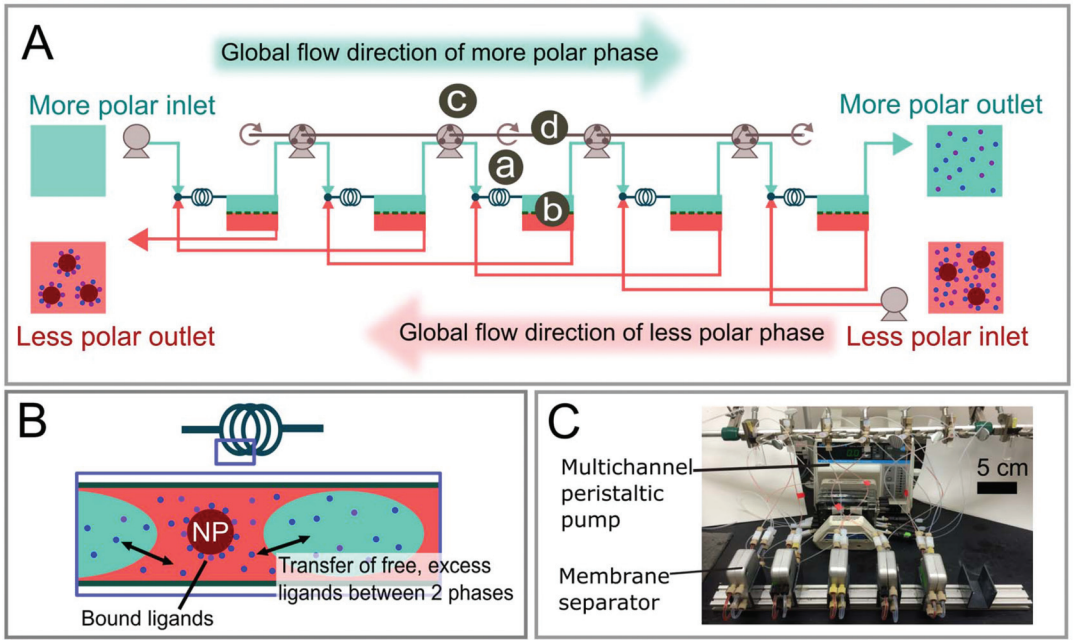

Fig. 1 (A) A scheme of a platform for 5-stage countercurrent extraction. Each stage, or module, comprises of (a) mass transfer tubing, (b) membrane separator. The more polar phase is delivered to a subsequent stage by (c) peristaltic pumping with multiple channels driven by (d) the same roller. (B) Drawing showing extraction of free ligands/precursors inside the mass-transfer tubing. The two phases form segmented flow. (C) Picture of the five-stage-LLE platform.

the tube is experimentally proven to be sufficient for complete mass transfer at the scale of interest.

The separation is achieved by the different wettability of the membrane by the two solvents (see Fig. S1 and S2† for the drawing and picture of the membrane separator with detailed description). By using a hydrophobic membrane, the less polar phase wets and permeates the membrane while the more polar phase is retained. To maintain successful separation, a fixed pressure difference between retentate and permeate sides is required ($\Delta P_{mem} = P_{mem}^{ret} - P_{mem}^{per}$).[21,22] Incorporation of a self-tuning pressure control diaphragm facilitates the use of the unit and isolates it from downstream pressure fluctuations.[23] This control element functions similarly to a dome-loaded pressure regulator in which an elastic film opens and closes a valve. To open the valve, the retentate has to build up pressure equal to ($P_{mem}^{per} + P_{dia}$), where P_{dia} is an additional specific pressure exerted by the diaphragm. With a suitable design, the film can provide P_{dia} to be within an operating window for ΔP_{mem}. In other words, ΔP_{mem} is self-tuned to P_{dia}, and decoupled from any downstream pressure fluctuations such as pumping between stages. In this work, ΔP_{mem} is estimated based on solvent properties and interfacial measurements (calculation available in ESI†). The combined effects of fast mass transfer (extraction) and complete separation result in a high percentage extraction at each individual module. The extraction can be improved further by cascading these modules into a multistage format.

The multistage extraction can be carried out in either crosscurrent or countercurrent fashions. For a small scale, the crosscurrent extraction (sequential washing) is more common owing to its simple setup. However, theoretically, the countercurrent extraction is more efficient than the crosscurrent extraction. As shown in Fig. 1, the previously described individual extraction stages are constructed into a multistage format. We connect them such that the two phases flow in opposite directions throughout the entire platform.[24] The more polar phase goes from stage 1 to stage N, and the other way around for the less polar phase. At any stage i, the two phases are mixed inside a T-mixer and then flow co-currently into the membrane separator. The two phases are separated and delivered to adjacent stages. The less polar phase permeates the membrane and flows to stage $i - 1$ by itself owing to the net pressure drop of the platform. On the other hand, the more polar phase is retained and delivered to stage $i + 1$ by peristaltic pumping. The pumping rate is set to be higher than the maximum flow rate of the retentate to avoid partial blockage to the flow.[25] Overall, it is important to emphasize that the flow inside each extraction module is co-current, but the net flows throughout the platform are countercurrent.

The capability of the LLE platform is demonstrated by two model nanocrystal case studies: (i) CdSe quantum dots (QDs) in octane, (ii) gold nanoparticles (Au NPs) in water. In the first system, CdSe QDs are prepared in a high-temperature and high-pressure tube reactor, utilizing octane as the solvent.[26] The cadmium and selenium precursors are cadmium oleate ($CdOA_2$) and trioctylphosphine selenide (TOPSe), respectively. Excess trioctylphosphine is used as a neutral ligand to improve the solubility of $CdOA_2$ in octane. Excess precursors and

Table 1 Experimental conditions for purification of CdSe QDs by LLE. The highlighted boxes indicate the changed variables in the comparative experiments

Experiment	A	B	C	D	E	F	G[a]
Solvent	ACN	DMF	MeOH	MeOH	MeOH	MeOH	MeOH
# of stages	1	1	1	3	5	5	5
S/F ratio	1	1	1	1	1	2	2

[a] Experiment G is done by cascading one additional stage to remove the residual methanol by ACN extraction.

ligands as well as byproducts generated during the synthesis remain in the crude CdSe QD solution and have to be removed by LLE. We examine systematically effects on separation efficiency by varying different process variables including solvent type, number of stages (N) and volumetric solvent-to-feed (S/F) ratio. Detailed experimental conditions are summarized in Table 1.

As shown in Fig. 2A, the absorption spectra of the CdSe QDs remain constant before and after the purification, indicating that LLE is non-destructive to the nanoparticles (TEM image of the purified CdSe QDs is available in ESI, Fig. S3†). The recovery yield (the amount of particles obtained after the purification divided by the amount of particles in the feed solution) is close to 100% in all conditions (calculation method in ESI and Fig. S4†). In Fig. 2B, the intensities of sharp peaks in the NMR spectrum significantly decrease after the multistage extraction, suggesting that the concentrations of the free ligands and impurities decrease. Similar phenomena are observed in ^{31}P NMR (Fig. S5†). The removal of ligands is also confirmed by TGA (Fig. S6†), where a significantly lower mass loss is detected in the LLE purified sample (Exp F) compared to the stock solution. In order to better compare the extraction performances under various conditions, the ligand population of each purified sample is quantified by ^{1}H NMR and the absorption spectrum.[27] The impurities are sorted into two groups: the OA and TOP species. The OA species include the excess cadmium precursor $CdOA_2$ and oleate-containing byproducts such as oleic acid. The TOP species represent the excess selenium precursor TOPSe, the excess ligands TOP and the byproduct trioctylphosphine oxide (TOPO). The OA species are calculated based on the NMR integral of the olefin region and the TOP species are determined by NMR integrals of the hydrocarbon region after subtracting the contribution from OA and the solvent. The lower level (0% removal) is estimated from the concentration of both species in the crude solution. The upper level (100% removal) is established by measuring the ligand population of CdSe QDs purified by gel permeation chromatography (GPC), which is known to be an effective method for isolating nanoparticles from impurities (Fig. S7†).[28]

We first study the effect of solvents, using a single extraction stage (N = 1) and S/F = 1. Acetonitrile (ACN), dimethyl formamide (DMF), and methanol (MeOH) are selected as the extraction solvents based on their immiscibility with octane at room temperature. MeOH yields effective extraction for both OA and TOP species while DMF only shows effective extraction on OA, and ACN barely removes impurities (Fig. 3). We also examine the scalability of this technique. By using CdSe QD solutions with different concentrations (13 μM and 80 μM), similar purification efficiencies are observed.

MeOH is known to be effective in removing $CdOA_2$ species during the precipitation/redissolution (PR) purification process, and can even replace the bound $CdOA_2$ species on the nanoparticle surface.[29,30] Compared to MeOH, DMF and ACN are considered as weak-coordinating or even non-coordinating solvents in the PR method, and are used in multiple PR cycles to avoid damage to the nanoparticles.[29–31] However, compared to the PR method, LLE is a significantly milder purification process (see quantum yield discussion in ESI†), and the

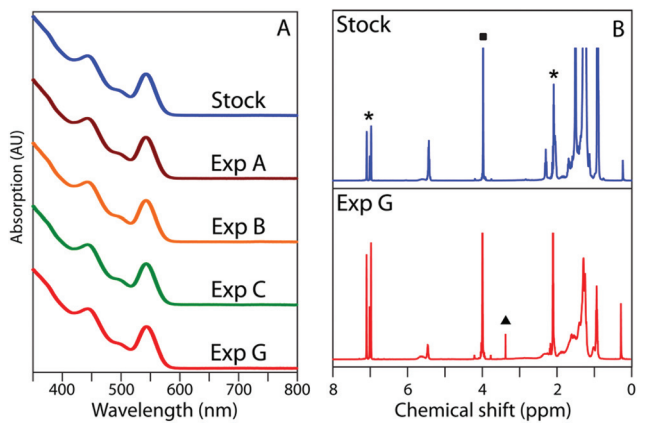

Fig. 2 (A) UV-Vis spectra of the stock and representing LLE purified samples. All the purified samples maintain their absorption characteristics after extraction. (B) ^{1}H NMR spectra of the CdSe stock solution and the LLE purified solution through experiment G. The marks in the spectra indicate peaks associated the NMR solvent toluene (asterisks), the internal standard ferrocene (square) and the extracting solvent methanol (triangle).

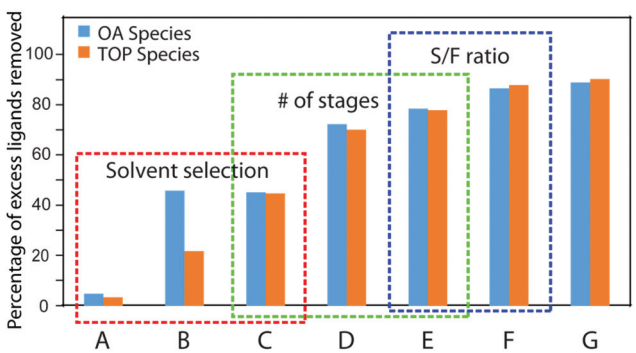

Fig. 3 Percent extraction of OA and TOP from CdSe QD feed solution with different operating conditions. The dashed boxes highlight the changed variable in the comparative experiments as described in Table 1.

extracting solvents are not directly in contact with the nanoparticles, which minimizes the risk of surface damage caused by the coordinating solvents.[11] Therefore, as the most effective extracting solvent, MeOH is chosen to be used for the later studies.

We also assess the effect of the number of stages (N). The amount of OA and TOP species removed from the crude solution increases with a larger number of stages (Fig. 3). The extraction gradually reaches its capacity as N becomes larger. Here, we also verify the reproducibility of our LLE technique. The percentage extraction of the ligands remains constant even after running this system for around 50 min (Fig. S8†), suggesting that continuous and reproducible nanoparticle purification can be achieved with the LLE platform.

To further enhance the degree of separation, we alter the S/F ratio. Increasing the S/F ratio from 1 to 2, the percentage extraction reaches 89% and 90% for OA and TOP, respectively. However, the MeOH and octane phases become miscible as the S/F ratio increases, especially with the presence of excess ligands at the interface. When we increase the S/F ratio to 5, CdSe QDs precipitate inside the mixing tubing as a result of the two phases becoming miscible under this condition (Fig. S9†). To achieve a higher capacity, other techniques should be incorporated into our platform. For example, an extracting agent, such as fatty amines, can be added to enhance the distribution coefficient of the ligands.[15]

As a final step, residual methanol content in the purified CdSe QDs octane phase is considered. As mentioned previously, methanol is known as a coordinating solvent to the CdSe QDs surface and the residual methanol may negatively affect any downstream processing of the nanoparticles such as shell growth or ligand exchange. Utilizing headspace chromatography (HS-GC), we are able to determine the methanol content in the octane phase after the extraction. For the best condition (Exp. F), the methanol content is 15.02 mg mL^{-1}. To remove the methanol, an additional stage of extraction is implemented such that the octane phase from the 5-stage extraction is mixed with a stream of ACN. ACN effectively removes the methanol, reducing the final methanol content down to 0.20 mg mL^{-1} (~99% methanol removed). As a non-coordinating solvent, the residual ACN content within the CdSe QDs octane phase is 12.32 mg mL^{-1}, which is likely to have negligible influence on later stage nanocrystal surface modification.

As a second demonstration of the LLE platform, we investigate the separation of excess thiol-PEG ligands from aqueous gold nanoparticle solution (Au NPs). As opposed to the CdSe QDs system in which the extraction is from nonpolar to polar organic phases, the extraction of the Au NP system is from aqueous to organic phase. Toluene is used as the extracting solvent. The absorption spectra of Au NPs remain constant before and after LLE, which suggests that there is no size or size distribution change of the NPs during purification (Fig. S10†). Thermogravimetric analysis (TGA) measures the feed and purified Au NPs in order to determine the fraction of thiols being removed. The smaller mass loss between 300 °C and 450 °C for the extracted sample indicates that LLE can also be used to purify thiol-PEG capped Au NPs (Fig. 4). If we attribute the entire mass loss between 200 °C and 500 °C to the removal of the organic ligand molecules from the system, then the organic/inorganic ratio decreases approximately 26% after extracting with toluene under the following condition: S/F = 2, T = 18 °C, N = 5. A TEM image of the Au NPs drop cast directly from the LLE solution reveals the discrete inorganic particles after purification (Fig. S11†).

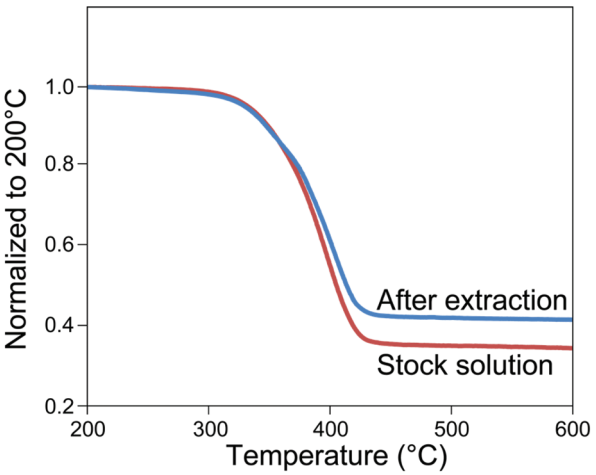

Fig. 4 TGA curves of the stock (red) and LLE purified (blue) thiol-PEG capped Au NPs. The curves have been normalized to 200 °C, where the solvent water has been completely removed.

Conclusions

We have successfully demonstrated continuous purification of nanocrystals using a multistage liquid–liquid extraction platform through two distinct systems: CdSe QDs in organic solvent and Au NPs in water. The effects of different process conditions such as extracting solvent type, number of stages and volumetric solvent-to-feed ratio have been examined systematically in this work. Using our method, we obtain highly purified nanoparticles with nearly complete recovery in a reproducible manner. This LLE platform opens up a new window for inline purification of nanoparticles as it has benefits of low energy/material consumption and high scalability compared to conventional methods. It can potentially be adapted with the flow synthesis of the nanocrystals so as to enable a fully continuous production of nanomaterials.

Acknowledgements

This work is supported by the National Science Foundation under grant no. ECCS-1449291. We thank Prof. Michael Strano and Prof. Alan Hatton of MIT for the use of the UV–Vis spectrometer and optical tensiometer in their laboratories.

Notes and references

1 O. Chen, H. Wei, A. Maurice, M. Bawendi and P. Reiss, *MRS Bull.*, 2013, **38**, 696–702.
2 G. Prieto, H. Tüysüz, N. Duyckaerts, J. Knossalla, G.-H. Wang and F. Schüth, *Chem. Rev.*, 2016, **116**, 14056–14119.
3 S. Raj, S. Jose, U. S. Sumod and M. Sabitha, *J. Pharm. BioAllied Sci.*, 2012, **4**, 186–193.
4 S. E. Skrabalak and R. L. Brutchey, *Chem. Mater.*, 2016, **28**, 1003–1005.
5 V. Sebastián and K. F. Jensen, *Nanoscale*, 2016, **8**, 15288–15295.
6 Z. Liu, K. Okabe, C. Anand, Y. Yonezawa, J. Zhu, H. Yamada, A. Endo, Y. Yanaba, T. Yoshikawa, K. Ohara, T. Okubo and T. Wakihara, *Proc. Natl. Acad. Sci. U. S. A.*, 2016, **113**, 14267–14271.
7 Y. Shen, A. Roberge, R. Tan, M. Y. Gee, D. C. Gary, Y. Huang, D. A. Blom, B. C. Benicewicz, B. M. Cossairt and A. B. Greytak, *Chem. Sci.*, 2016, **7**, 5671–5679.
8 M. Abolhasani, C. W. Coley, L. Xie, O. Chen, M. G. Bawendi and K. F. Jensen, *Chem. Mater.*, 2015, **27**, 6131–6138.
9 I. Lignos, S. Stavrakis, G. Nedelcu, L. Protesescu, A. J. deMello and M. V. Kovalenko, *Nano Lett.*, 2016, **16**, 1869–1877.
10 S. A. Khan and S. Duraiswamy, *Lab Chip*, 2012, **12**, 1807–1812.
11 Y. Shen, M. Y. Gee and A. B. Greytak, *Chem. Commun.*, 2017, **53**, 827–841.
12 D. Kim, H. K. Park, H. Choi, J. Noh, K. Kim and S. Jeong, *Nanoscale*, 2014, **6**, 14467–14472.
13 H. Lim, J. Y. Woo, D. C. Lee, J. Lee, S. Jeong and D. Kim, *Sci. Rep.*, 2017, **7**, 43581.
14 S. F. Sweeney, G. H. Woehrle and J. E. Hutchison, *J. Am. Chem. Soc.*, 2006, **128**, 3190–3197.
15 Y. Yang, J. Li, L. Lin and X. Peng, *Nano Res.*, 2015, **8**, 3353–3364.
16 K. Wang and G. Luo, *Chem. Eng. Sci.*, DOI: 10.1016/j.ces.2016.10.025.
17 A. Holbach and N. Kockmann, *Green Process. Synth.*, 2013, **2**, 157–167.
18 Y. Zhao, G. Chen and Q. Yuan, *AIChE J.*, 2006, **52**, 4052–4060.
19 M. N. Kashid, I. Gerlach, S. Goetz, J. Franzke, J. F. Acker, F. Platte, D. W. Agar and S. Turek, *Ind. Eng. Chem. Res.*, 2005, **44**, 5003–5010.
20 I. Vural Gürsel, S. K. Kurt, J. Aalders, Q. Wang, T. Noël, K. D. P. Nigam, N. Kockmann and V. Hessel, *Chem. Eng. J.*, 2016, **283**, 855–868.
21 A. Günther, M. Jhunjhunwala, M. Thalmann, M. A. Schmidt and K. F. Jensen, *Langmuir*, 2005, **21**, 1547–1555.
22 J. G. Kralj, H. R. Sahoo and K. F. Jensen, *Lab Chip*, 2007, **7**, 256–263.
23 A. Adamo, P. L. Heider, N. Weeranoppanant and K. F. Jensen, *Ind. Eng. Chem. Res.*, 2013, **52**, 10802–10808.
24 M. Peer, N. Weeranoppanant, A. Adamo, Y. Zhang and K. F. Jensen, *Org. Process Res. Dev.*, 2016, **20**, 1677–1685.
25 N. Weeranoppanant, A. Adamo, G. Saparbaiuly, E. Rose, C. Fleury, B. Schenkel and K. F. Jensen, *Ind. Eng. Chem. Res.*, 2017, **56**, 4095–4103.
26 L. Xie, Y. Shen, D. Franke, V. Sebastián, M. G. Bawendi and K. F. Jensen, *J. Am. Chem. Soc.*, 2016, **138**, 13469–13472.
27 Z. Hens and J. C. Martins, *Chem. Mater.*, 2013, **25**, 1211–1221.
28 Y. Shen, M. Y. Gee, R. Tan, P. J. Pellechia and A. B. Greytak, *Chem. Mater.*, 2013, **25**, 2838–2848.
29 A. Hassinen, I. Moreels, K. De Nolf, P. F. Smet, J. C. Martins and Z. Hens, *J. Am. Chem. Soc.*, 2012, **134**, 20705–20712.
30 B. Shakeri and R. W. Meulenberg, *Langmuir*, 2015, **31**, 13433–13440.
31 N. C. Anderson, M. P. Hendricks, J. J. Choi and J. S. Owen, *J. Am. Chem. Soc.*, 2013, **135**, 18536–18548.